J. Biochem. **135**, 337–346 (2004)
DOI: 10.1093/jb/mvh041

pH-Induced Conformational Transition of *H. pylori* Acyl Carrier Protein: Insight into the Unfolding of Local Structure

Sung Jean Park, Ji-Sun Kim, Woo-Sung Son and Bong Jin Lee*

National Research Laboratory (MPS), Research Institute of Pharmaceutical Sciences, College of Pharmacy, Seoul National University, San 56-1, Shillim-Dong, Kwanak-Gu, Seoul 151-742, Korea

Received December 2, 2003; accepted January 6, 2004

Acyl carrier protein (ACP) is a small acidic protein and its primary structure is highly conserved in various bacterial sources. Despite its small size, it interacts with diverse proteins associated with many biosynthetic pathways. The three-dimensional structure of *H. pylori* ACP and its structural characteristics were clarified using NMR and CD spectroscopy. *H. pylori* ACP consists of four helices connected by different sized loops. The helices correspond to residues L3-Q14 (αI), S36-G50 (αII), D56-E60 (αIII), and V65-K76 (αVI). The size of each helix differs slightly from that of homologous ACPs. However, *H. pylori* ACP showed a distinct pH-dependent conformational characteristic: at neutral pH, it adopts a partially unfolded structure, while it has a tight fold at pH 6. The chemical shift perturbation and ^{1}H-^{15}N steady state NOE analysis at both pH 6 and 7 showed that the local change of structural components occurred mainly around loop II, and this change was reflected by the changes of the residues Ile 54 and Asp 56. Examination of the structure showed that the network of Glu 47, Ile 54, Asn 75, and Lys 76 is very important for the structural stability. The pH-dependent folding process shows a kind of cooperativity, since all the residues involved in the conformational transitions are contiguous and in spatial proximity.

Key words: ACP, circular dichroism, *H. pylori*, NMR.

Acyl carrier protein (ACP) found in bacteria is a monofunctional protein, that is, the type II enzyme in fatty acid biosynthesis; but by using its ability to transfer acyl groups, it interacts with diverse proteins associated with fatty acid biosynthesis (*1*), membrane-derived oligosaccharide biosynthesis (*2*), activation of protein toxins (*3*), synthesis of polyketide antibiotics (*4*), and synthesis of rhizobial nodulation signaling factors (*5*). Thus, it is not surprising that ACP has been investigated extensively. All the ACPs are decorated by acyl carrier protein synthase (ACPS) with fatty acids, which are covalently attached as thioesters to the 4′-phosphopantetheine prosthetic group at highly conserved Ser 36 (*6*). Fatty acid binding has little influence on ACP conformation under physiological conditions (*7*), but it stabilizes ACP against denaturation at alkaline pH (*8–10*).

The one of main topics in ACP studies is the functionally and structurally crucial residues that allow ACP to manifest a diversity of functions despite its highly conserved primary structure. Some studies showed the relationship between mutation of residues and pH-dependant structural stability. The mutation of Val 43 to Ile in *E. coli* ACP increases the stability to pH-induced expansion in eletrophoretic systems, concomitantly inducing more compact folding (*11*). The mutants F50A and I54A of *V. harveyi* are incapable of adopting a native conformation with increased hydrodynamic radius at neutral pH (*12*). In addition, a few basic residues scattered near the N- and C-termini, for example, His 75 of *E. coli* ACP, are necessary for ACP to maintain a native conformation at neutral pH (*13*). Together with these mutation analyses, ACP and complex structures determined by NMR or X-ray crystallography (*14–23*) provide insights into the putative role of each structural component involved in heterologous protein interactions. Although the binding modes of protein interactions are diverse, helices II and III of ACP seem to be principally involved in formation of a complex. For example, the contacts between acylated-ACP and ACPS of *E. coli* are predominantly hydrophilic in nature, with almost all interactions occurring between helix I of ACPS and helix III of ACP. This contact is locked by residues Leu 37 and Met 44 in helix II of ACP *via* hydrophobic interaction with ACPS and by residues Asp 35, Asp 38, Glu 41, and Asp 48 *via* salt bridging or hydrogen bonding with ACPS (*22*). The complex formation of β-ketoacyl-acyl carrier protein synthase III (FabH) and ACP of *E. coli* is mediated by helix II of ACP, in which the interactions of Glu 41 and Ala 45 are important (*23*). In the activation process of *E. coli* hemolysin toxin (HlyA), ACP specifically interacts with an internal protein acyltransferase (HlyC) through Ser 27, Val 29, Gly 33, Glu 41, Val 43, Glu 48, Ile 54, Asp 56, and Lys 61 corresponding to a long region, loop I-helix II-loop II-helix III of ACP (*24*). However, the nature of the proper recognition and precise alignment between the protein moieties of ACP and its various interactive proteins is not fully understood, although the highly conserved residues are thought to be responsible for the interactions between ACP and various proteins (*24*).

H. pylori ACP is composed of 78 amino acids with a pI value of 3.9, and its primary structure is similar to those of homologuous ACPs. However, it shows an unusual

*To whom correspondence should be addressed. Tel: +82-2-880-7869, Fax: +82-2-872-3632, E-mail: lbj@nmr.snu.ac.kr

behavior in CD spectra at neutral pH (see below). To clarify the pH-dependent conformational transition and identify which residue plays a central role in the structural change, here we determined the three-dimensional structure of *H. pylori* ACP by NMR and investigated the contribution of structural components to maintaining stability at different pHs.

MATERIALS AND METHODS

Materials—A genomic DNA from *H. pylori* (ATCC 700392) was obtained from ATCC (Manassas, VA, USA). Restriction endonucleases were purchased from New England Biolabs (Beverly, MA, USA) and Promega (Madison, WI, USA). Cloned *Pfu* DNA polymerase was obtained from Stratagene (La Jolla, CA, USA). All materials were of reagent or biotechnological grade.

Protein Expression and Purification—H. pylori ACP (HP0559, 78 a.a) was cloned from a genomic DNA of *H. pylori* using PCR and placed into a pET 21a vector. PCR amplification was performed with *pfu* DNA polymerase using two overlapping primers, 5′-GGAATTCCATATGGCTTTATTTGAAGATATTCAGGC-3′ (sense, *Nde*I) and 5′-CCGCCGCTCGAGTGAAGCCAGTTTATTATCCTCAATATACTT-3′ (antisense, *Xho*I) containing the restriction enzyme sites (underlined). Recombinant ACP, uniformly labeled with ^{15}N (>95%) or ^{15}N (>95%) and ^{13}C (>95%), was expressed in *E. coli* strain BL21 (DE3). After incubation at 37°C for 7 h, protein expression was induced by adding IPTG to a final concentration of 1 mM. At 4 h postinduction at 37°C, cells were harvested by centrifugation with 8,000 rpm at 4°C for 15 min (Beckman J2-MC). The bacterial cell pellet was suspended in 100 ml of the lysis buffer [50 mM Tris-Cl (pH 7.9), 0.5 M NaCl, 10% glycerol, and 0.1 mM PMSF]. The bacterial lysis was performed by sonication (4 × 30-s pulses) until the lysate became clear. After lysis, the supernatant was applied to a His-tag column (2.5 × 20 cm). Bound ACP was eluted with a linear 50–500 mM immidazole gradient at the flow rate of 1 ml/min. After pooling the selected fractions, the mixture was purified by a Hiprep™ 16/10 DEAE FF column (Amersham Pharmacia Biotech, Uppsala, Sweden). The purified protein was treated with 100 mM DTT at 37 °C overnight to remove acyl chains (*21*). The DNA of the expression clone was sequenced and the purity of the proteins determined by SDS-PAGE and mass spectrometry.

Circular Dichroism—Circular dichroism (CD) analysis was performed with a Jasco J-715 spectropolarimeter at 20°C. Purified *H. pylori* ACP was dialyzed against 5 mM potassium phosphate buffer (pH 7.4) supplemented with 1 mM EDTA and 1 mM DTT. For pH-titration, the pH of each sample was adjusted with 0.1 N HCl. CD measurements were carried out in a wavelength range between 190 nm and 250 nm. The resultant spectra were corrected for the buffer signal. To investigate the thermodynamic properties of ACP, temperature scan was performed at 222 nm in a temperature range between 12°C and 90°C. The rate of temperature ramping was 1 °C/min.

NMR Spectroscopy—NMR spectra were acquired on a Bruker AVANCE 600 MHz spectrometer at 303 K. The spectra recorded on ^{15}N-labelled ACP were 2D ^{15}N-HSQC (*26*); 3D ^{15}N-NOESY-HSQC (*27*); 3D ^{15}N-TOCSY-HSQC (*28*); 3D HNHA (*29*); {^{1}H}-^{15}N steady-state NOE. For the measurement of conformational differences at pH 6.0 and pH 7.4, ^{15}N-HSQC (2048 t1 × 256 t2), {^{1}H}-^{15}N steady-state NOE (2048 t1 X 256 t2), and ^{15}N-TOCSY-HSQC (1024 t1 × 64 t2 × 256 t3) were obtained at each pH. The spectra recorded on ^{15}N/^{13}C-labelled samples were 3D HNCA, 3D HNCO, 3D HN(CO)CA, (*30*); 3D HNCACB (*31*); 3D HN(CO)CACB (*32*). Unless indicated otherwise, all *H. pylori* ACP samples were dissolved in 90% H_2O/10% $^{2}H_2O$, containing 500 mM NaCl, 50 mM potassium phosphate, 10 mM DTT, 1 mM EDTA, at pH 6.0. The monomer concentration of the ACP ranged between 2 and 4 mM. A mixing time of 100 ms was used in all NOE experiments (1024 t1 × 64 t2 × 256 t3). The 3D ^{15}N-edited TOCSY-HSQC employed a mixing time of 50 ms. Chemical shift calibrations for all nuclei were performed relative to the proton resonance of DSS as suggested previously (*33*). Spectra were processed with NMRPipe (*34*) and analysed with NMRView 5. The sequence-specific resonance assignment was carried out using standard procedures (*35*). Secondary structure predictions were made from an analysis of the ^{13}Cα, ^{13}Cβ, and ^{13}C′ chemical shifts using the CSI program of Wishart and Sykes (*36*).

Structure Calculation—The NMR solution structure is based on interproton distance restraints converted from observed NOEs in both the ^{15}N-edited NOESY and ^{13}C-edited NOESY experiments. The NOE intensities were classified as either strong (1.8–2.7 Å), medium (1.8–3.3 Å), or weak (1.8–5.5 Å) restraints. The upper limits for distances involving methyl protons and nonstereospecifically assigned methylene were corrected appropriately for sum averaging, and an additional 0.5 Å was added to the upper distance limits for NOEs involving methyl protons averaging. ϕ and φ torsion angle restraints were obtained from ^{15}N, Hα, C, and Cβ chemical shifts using the TALOS program, in which only "good" predictions were used to generate a restraint (*16*). The ACP polypeptide chain used for the NMR structural analysis contains 86 residues, including 8 nonnative residues (LEHHHHHH) at the C terminus. The 8 C-terminal residues were not used in the structure calculation, since these residues are essentially unstructured, which is evidenced by the small number of NOE cross-peaks. The structure of ACP was determined from a total of 1115 distance restraints and 81 torsion angles constraints comprised of 41 ϕ and 40 ψ dihedral restraints. In addition, 21 J-coupling restraints obtained from the HNHA spectrum were incorporated into the calculation. The structures were calculated using the program CNS. An iterative procedure was used to successively introduce an increasing number of NOE distance restraints. For the initial rounds of structure calculations, manually assigned NOEs were used as input restraints. Each round started with 20 random conformers, from which the 10 with the lowest target function were used to analyze constraint violations and assign additional NOE constraints in CNS for the following round of refinement. This process was repeated until more than 90% of the cross peaks in the ^{15}N-edited NOESY and ^{13}C-edited NOESY spectra had been assigned and all consistent violations were eliminated. A final ensemble of 20 structures contained no distance restraint violations greater than 0.2 Å, and no torsion angle restraint violations greater than 2° were obtained.

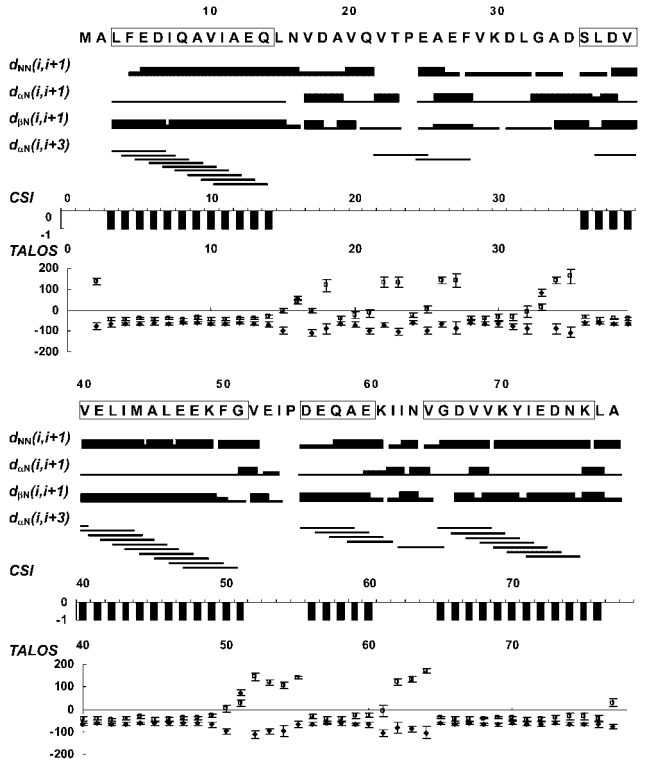

Fig. 1. **Summary of structural information obtained from NMR spectra at pH 6.0, 30°C.** The sequential NOE connectivities d_{NN}, $d\alpha_N$, and $d\beta_N$ are indicated by horizontal bars; the thickness of each bar is proportional to the NOE intensity. The medium range connectivity $d\alpha_N$ (*i, i+3*) is shown by lines starting and ending at the positions of the residues related by the NOE. The negative vertical bars indicate helical region calculated by the CSI. Φ and ψ angle values are predicted by TALOS. The predicted helical regions are represented by boxes.

All subsequent analyses of the structure were performed using MOLMOL and PROCHECK-NMR.

RESULTS

Structure of H. pylori ACP—The structure of *H. pylori* ACP was investigated by multidimensional NMR spectroscopy. We previously had reported only the backbone assignments of apo *H. pylori* ACP (*37*). The assignments comprise 97% of all ^{1}HN, ^{15}N, ^{13}CO, ^{13}Cα and ^{13}Cβ resonances covering 74 of the 76 non-proline residues. On the basis of resonance assignments, four helical regions were clearly identified using the program CSI (*36*). These correspond to residues L3-Q14 (αI), S36-G51 (αII), D56-E60 (αIII), and V65-K76 (αVI). The CSI result is clearly consistent with the distribution of NOEs as shown in Fig. 1. Generally, a NOE pattern of a helical region shows strong $d_{bN}(i, i+1)$, medium $d_{NN}(i, i+1)$, weak d_{aN} $(i, i+1)$, and weak d_{aN} $(i, i+3)$ (*38*), which is consistent with the four helices of *H. pylori* ACP. The backbone (Φ, Ψ) angles analysis using TALOS (*39*) showed 55 residues are predicted as good agreement. Especially, all the residues of four helical regions except Lys 49 and Asn 75 were defined as good agreement and the deviations of (Φ, Ψ) angles of residues involved in loop regions were large, which shows the secondary structure analyzed is correct.

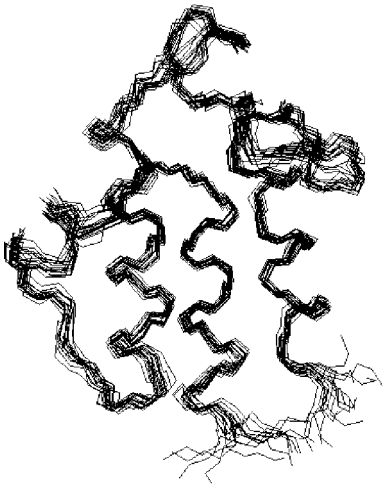

Fig. 2. **Ensemble of 20 torsion angle dynamics conformers of *H. pylori* ACP after alignment of the backbone atoms of residues 3–76.** The backbone N, Cα, and C′ atoms are shown.

Based on the information of secondary structure, the three-dimensional structure was determined by CNS. The calculation employed 1123 nontrivial NOE upper limit distance constraints and 102 torsion angles restraints. The ensemble of 20 structures resulting from the final stage of refinement is shown in Fig. 2. The helical regions accord well with the predicted secondary structure, while Gly 51 is not included in helix II, since the βN(50, 51) NOE was observed with weak intensity and the (Φ, Ψ) angles were largely different from those of the other components in helix II. The NMR structure is well defined, and superposition of residues 3–76 on the mean structure yields rmsd values of 0.78 ± 0.09 and 1.21 ± 0.12°C for backbone atoms and non-hydrogen atoms, respectively. Another measure of structure quality is provided by Ramachandran analysis of the ensemble, which places 80.3 % of the residues in the most favored regions, 16.8% in additional allowed regions, 1.7% in generously allowed regions, and 1.2% in disallowed regions. Structural statistics for the family and the average structure are summarized in Table 1.

The structures of the homologous ACPs originating from other bacterial sources were previously reported by NMR or X-ray crystallography (*14–21*). Compared to *E. coli* and *B. subtilis* ACPs, *H. pylori* ACP consists of a medium-sized helix I which is shorter than that of *B. subtilis* ACP and longer than that of *E. coli* ACP, well-conserved helix II, an equal or longer helix III and a longer helix IV (Fig. 3). Like other ACPs, *H. pylori* ACP would form a helical bundle structure through hydrophobic contacts between helices. The residues involved in this interaction correspond to L3, F4, I7, V10, I11, and Q14 in helix I; V39, L42, I43, and L46 in helix II; and V65, A68, V69, and I72 in helix IV. The orientation of each helix is mainly maintained by interactions of these residues. The long loop I is not well ordered because of deficiency of medium- and long-range NOEs. However, it serves as a frame maintaining the up-down-down topology of helices through hydrophobic interactions of several residues with helices: L15, V22, T23, A26, and F28 interact with Q8, I11, and L14 in helix I; L42 in helix II; and V65 in

Table 1. **Restraints and statistical analysis of structures.**

Experimental restraints	
Interresidue NOEs[1]	740
Intraresidue NOEs	375
J-coupling restraints[2]	21
Dihedral angle restraints[3]	81
Structural statistics	
Maximum violation	
Distance (Å)	0.12
Angle (°)	1.21
R.m.s deviations from ideal geometry	
Bonds (Å)	0.0014 ± 0.00008
Angles (°)	0.307 ± 0.0054
Impropers (°)	0.1433 ± 0.0106
Ramachandran analysis (%)[4]	
Residues in most favored regions	80.3
Residues in additional allowed regions	16.8
Residues in generously allowed regions	1.7
Residues in disallowed regions	1.2
Coordinate precision (Å, residues 3–76)	
Backbone	0. 78
Heavy atoms	1.21
Energetics (kcal/mol)[5]	
E_{total}	68.03 ± 4.6
E_{bond}	2.36 ± 0.27
E_{angle}	31.81 ± 1.13
$E_{improper}$	1.83 ± 0.28
E_{vdw}	18.49 ± 2.14
E_{noe}	8.65 ± 1.44
E_{coup}	4.88 ± 2.73
E_{cdih}	0.01 ± 0.01

Statistical analyses are conducted for 20 of the lowest-energy structures of 100 structures calculated. [1]NOEs were classified by relative intensity, with either strong (1.8–2.7 Å), medium (1.8–3.3 Å), or weak (1.8–5.5 Å) restraints. [2]HN-Hα J-coupling values were obtained by analysis of 3D HNHA spectra and used as a direct periodic restraint in CNS based on the Karplus relationship. [3]Dihedral angle restraints were obtained either by chemical shift analysis using TALOS or by repeated occurrence in Ramachandran-allowed regions in unrestrained structures. [4]Ramachandran statistics were calculated using PROCHECK-NMR and exclude Pro, Gly and terminal residues. [5]The default parameters and force constants of protein-allhdg.param and anneal.inp in CNS 1.1 were used for calculation.

helix IV. In addition, I54 in loop II connecting helix II and III significantly contributes to stabilization of the main helical core by interacting with E47, V52, V69, Y71, N75, K76. The overall folding of ACPs is similar, as shown in Figure 4a and 4b. However, variations in the structures are apparent in the loop regions, and the relative position of helix I, III, and IV compared to helix II of *H. pylori* ACP is somewhat different from that of other ACPs (Fig. 4c). This topological difference, indicating that these ACP structures are relatively unique, may be caused by variation of loop regions and helix lengths.

Conformational Transition of H. pylori ACP at Various pHs; CD Studies—The effect of pH on the structural stability was measured using CD spectroscopy (Fig. 5). *H. pylori* ACP undergoes remarkable structural change with change in pH. As the pH increased, the absolute value of intensities at 208 nm and 222 nm decreased and the negative minimum at 208 nm shifted toward 205 nm, indicating that at neutral and alkaline pH the conformational transition of ACP occurred (Fig. 5a). The partially unfolded state at pH 7 is a unique characteristic of *H. pylori* ACP. It was shown that the overall helical structure of *E. coli* ACP was maintained at pH 7 (*40*). In contast, *V. harveyi* ACP exhibited a random coil-like conformation at pH 7 (*12*). Therefore, it seems likely *H. pylori* ACP adopts a distinct conformation at neutral pH which is different from those of *E. coli* ACP and *V. harveyi* ACP. It was suggested that the structural difference between *E. coli* ACP and *V. harveyi* ACP at neutral pH may be caused by the acidic character of the proteins (*12*). Interestingly, *H. pylori* ACP is predicted to have overall negative charge of –19, which lies between that of *E. coli* (–18) and *V. harveyi* (–22). The apparent pI value of *H. pylori* ACP seems to be around 4, since the protein aggregated and precipitated at pH 4, which is consistent with the calculated pI, 3.9. Thermodynamic property of *H. pylori* ACP, as expected, revealed the presence of two clear conformational states depending on pH (Fig. 5b). At the acidic pH 6, the temperature curves of the *H. pylori* ACP showed a distinct melting temperature around 50°C, which is a general characteristic of a tightly folded protein. However, the curves at neutral and basic pHs are largely different: in the range between 12°C and 25°C, they decreased. This effect was inverted as temperature increased toward 50°C. Above 50°C, the slight intensification of the CD signal occurred again. This unusual behavior suggests that the unfolding process above neutral pH proceeds through multi-phasic changes, in at least three stages. The second and third stage changes occur between 25°C and 90°C and seem to be a process of denaturation and non-specific aggregation. However, it is not clear whether the unique initial intensification between 12°C and 25°C is derived from the intermolecular or intramolecular interactions. To verify the contribution of ionic strength to the therymodynamic property, the salt concentration dependence of *H. pylori* ACP stability was evaluated at pH 6 and 7. The thermal stability, like that of *E. coli* ACP (*41*), increased with increasing salt concentration at pH 6 (Fig. 5c). By contrast, at pH 7, the pattern and intensity of Tm curves were not significantly changed even at 500 mM NaCl (Fig. 5d). It is well

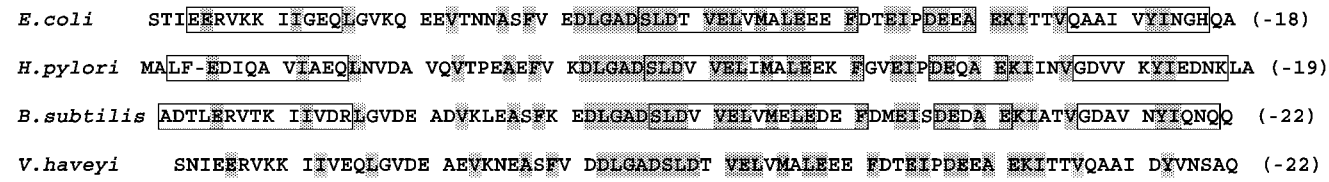

Fig. 3. **Comparison of secondary structures of ACPs.** The helix regions are represented by boxes. Identical amino acids are indicated by dark gray. The numbers at the end of sequences are the numbers of negatively charged residues (Glu and Asp) at neutral pH.

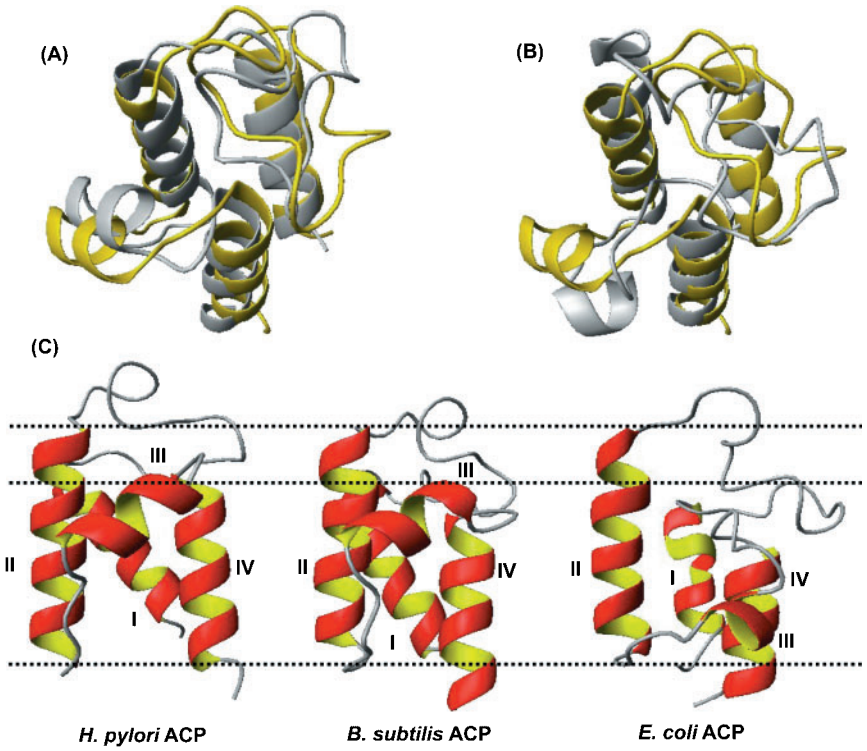

Fig. 4. **Comparison of the *H. pylori* ACP structure with the *B. subtilis* ACP and *E. coli* ACP structures.** The ribbon diagram of the average structure of the 20 best structures of *H. pylori* ACP was compared with the average models for *B. subtilis* ACP and *E. coli* ACP obtained from the Brookhaven Protein Data Bank. (A) Superposition of the *H. pylori* ACP structure (gold) with the *B. subtilis* ACP structure (light gray) (B) Superposition of the *H. pylori* ACP structure (gold) with the *E. coli* ACP structure (light gray) (C) The helices show topological differences, while the overall folds are very similar. The dotted lines are included for comparison of relative spatial positions between helices.

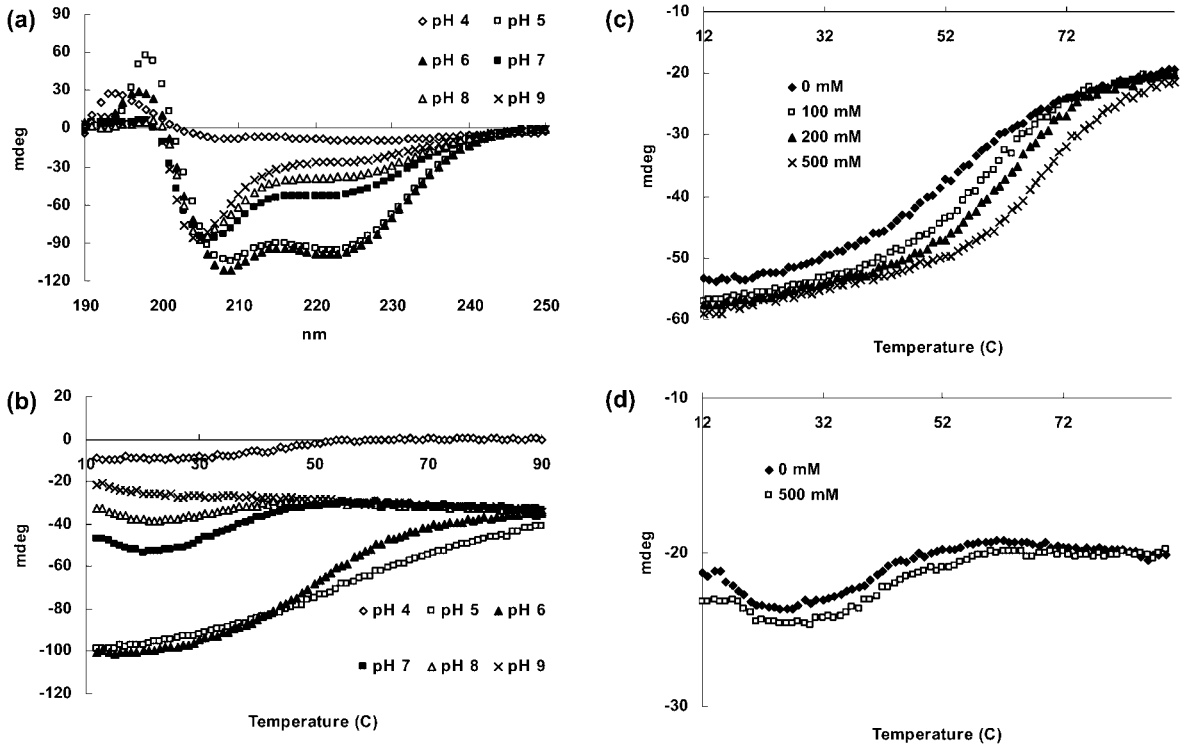

Fig. 5. **(a) CD spectra recorded at various pHs in 5 mM potassium phosphate buffer supplemented with 1 mM EDTA and 1 mM DTT.** (b) Tm curves of *H. pylori* ACP. Temperature scan was performed at 222 nm in a temperature range between 12°C and 90°C. (C) The effect of salt (NaCl) on the structural stability was evaluated by observation of shift of Tm value with increasing salt concentration at pH 6. (d) Tm curves of *H. pylori* ACP at pH 7 with increasing salt concentration.

documented that, at pH 7, monovalent salts non-specifically stabilize ACP by decreasing electrostatic repulsion of negatively-charged proteins (*13*, *41*). However, this masking effect of salt was not applicable to *H. pylori* ACP at pH 7, which indicates the core elements for maintaining the tertiary fold were partially disrupted by pH elevation.

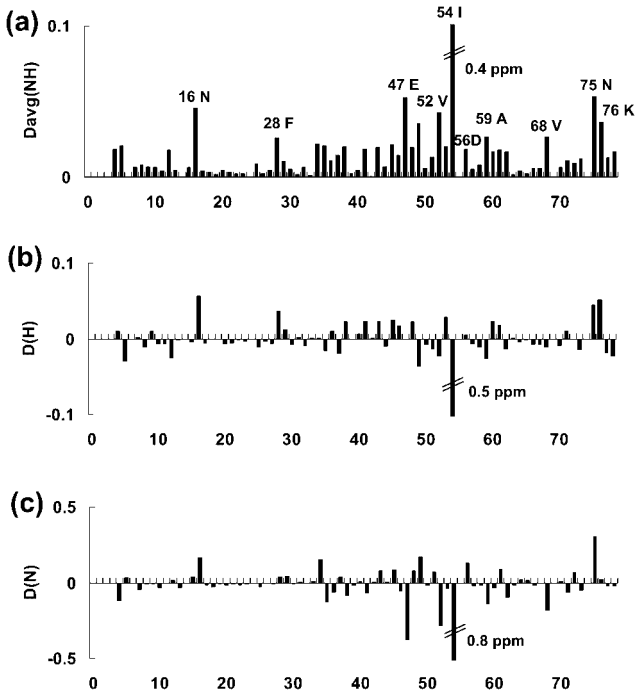

Fig. 6. **Chemical shift differences with varying pH.** The ^{1}H and ^{15}N chemical shifts at pH 7 were subtracted from those at pH 6. The unit of *Y* axis is ppm, and that of the *X* axis is residue number. The intensity of Asp 56 extensively decreases at pH 7. However, at the lowest contour level of the spectrum, the peak of Asp 56 can be found with low intensity. The chemical shift change of Asp 56 was calculated using this peak. (a) The weighted-averaged chemical shift differences, $\Delta_{avg}(HN) = \{[(\Delta H)^2 + (\Delta N/5)^2]/2\}^{1/2}$. The symbol Δ is replaced with D on the graphs. (b) Chemical shifts differences of amide proton (c) Chemical shifts differences of amide nitrogen.

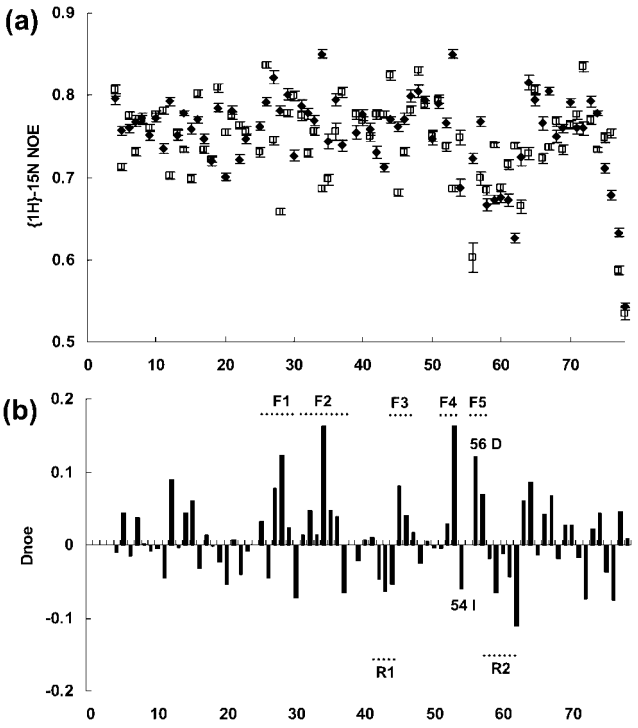

Fig. 7. **^{1}H-^{15}N steady state NOE analysis at pH 6 and pH 7.** The numbers on the X axis represent the position of residues. (a) Hetero NOE values are recorded at pH 6 (diamonds) and pH 7 (squares). Error bars are indicated on each NOE. (b) The NOE differences (Dnoe) were calculated by subtracting the NOE values at pH 7 from those at pH 6. R1 and R2 are the regions exhibiting negative NOE differences and thus of restricted motion; F1–F5 are regions exhibiting positive NOE differences implying high flexibilities with increasing pH.

Conformational Transition of H. pylori ACP; NMR Studies Based on Chemical Shift Perturbation and ^{1}H-^{15}N Steady-State NOE Analysis—To clarify the pH effect on the structure of *H. pylori* ACP, the chemical shift perturbation was observed by ^{15}N-^{1}H HSQC spectrum. Spectra measured at pH 6.0 and pH 7 were compared and the chemical shift differences were weighted-averaged by the previously reported method (*42*, Fig. 6). Calculated differences exceeded 0.1 ppm only in the case of Ile 54, whose chemical shift varied up to 0.4 ppm (Fig. 6a). The change of Ile 54 is a downfield shift in both axes, ^{1}H and ^{15}N. Interestingly, Glu 47, of which the side chain is buried in hydrophobic core, unlike in other ACPs, and is extruded toward loop II containing Ile 54 (*17–21*), showed the same downfield shift. In addition, the peak intensity of Asp 56 decreased sharply to only 1% of the peak intensity at pH 6 (data not shwon). To verify whether these differences reflect the conformational transition of *H. pylori* ACP, information on the backbone motions of the individual NH vectors was obtained through ^{1}H-^{15}N heteronuclear NOEs (Fig. 7). The values of each residue at pH 6 are primarily above 0.7 (the average value of all NOEs is 0.75), indicating that a well-ordered structure exists. Interestingly, compared with other regions, the region between the Gln 58 and Ile 62, including a part of helix III, has lower NOE values, averaging 0.66. This result implies that the backbone NH vectors around helix III are relatively fluctuating in the folded state. The long loop I connecting helices I and II showed unexpectedly high values of NOEs, despite the large number of residues. When the dynamic mobility of the backbone was measured at pH 7, the NOE values changed broadly along the polypeptide chain (Fig. 7a). The relatively flexible region, Gln 58–Ile 62 at pH 6 showed an increased NOE value of 0.71, indicating that this area comes into close contact with other structural components. The averaged NOE value of all residues was 0.74, which superficially implies that pH does not significantly affect the structural mobility. However, some residues, including Phe 28, Ala 34, Glu 53, Asp 56, and Ile 62, whose values of differences are above 0.1, showed notable changes. To clearly show the changes of NOEs, the differences of NOE values of each residue are calculated (Fig. 7b). The absolute values of differences were not large, but a distinct pattern of positive and negative NOE differences can be observed. Assuming that a group composed of at least three residues of similar motional properties in close vicinity may be taken to define a local structure, regions of restricted motions (R1–R2), and regions of flexibilities (F1–F5) are identified with the elevation of pH (Fig. 7b). R1 and R2 correspond to residues 42–44 in helix II and 58–62 in helix III and loop III, respectively, while F1, F2, F3, F4, and F5 correspond to residues 27–29 in loop I, residues 31–36 in loop I, residues 45–47 in helix II,

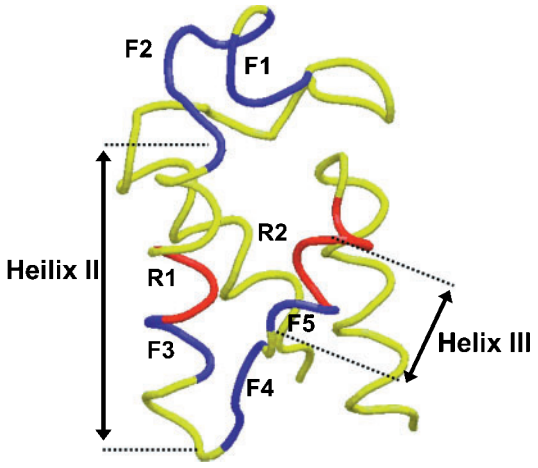

Fig. 8. **Schematic representation showing regions of altered flexibility by pH variation.** Regions of restricted motion (R1–R2) are represented in red, and regions of flexibilities (F1–F5) in blue.

52–53 in loop II, and 56–57 in helix III, respectively. Note that F4 and F5 have only two residues, but these were included because of the large magnitude of the NOE difference. These variable regions are represented in the three-dimensional structure (Fig. 8). As shown in Figure 8, the regions of restricted motions (R1–R2) and flexibilities (F1–F5) are all spatially in close proximity and mainly located around loop II. Therefore, the change of secondary structure may primarily occur in helices II and III, and loop II may play a critical role in maintaining the whole structure. It is noteworthy that the residues involved in the conformational transitions are contiguous, suggesting a kind of cooperativity in the folding process. Residue Ile 54 in loop II shows a distinct alteration in chemical shift perturbation and appears to have a slightly restricted motion at pH 7 (Fig. 7b). The analysis of 3D ^{15}N-edited NOESY spectrum revealed Ile 54 interacts with the residues Met 44 and Glu 47 in helix II, Val 52 in loop II, Ala 59 in helix III, and Val 68 in helix IV, because of the presence of NOEs between side-chain and amide protons (Fig. 9). Also, a detailed examination of the NOESY spectrum obtained at pH 6 revealed that clear NOE connectivities can be seen between γN protons of Asn 75 and methyl protons of Ile 54. These residues showed notable changes in chemical shift perturbation, as shown in Fig. 6, and, except for Val 68 and Asn 75, they are included in the regions of flexibility or rigidity around loop II (Fig. 7). This observation strongly indicates the Ile 54 is a key residue in cooperative unfolding of *H. pylori* ACP. The extensively decreased intensity of resonance of Asp 56 should be related with the increased flexibility (Fig. 7b), which indicates the conformation of helix III is easily exchangeable at neutral pH. Note that the NOE value of Asp 56 could not be determined from the spectra at a normal contour level. However, at the lowest level, the peak of Asp 56 could be detected with low intensity, and this peak was used to calculate the NOE value.

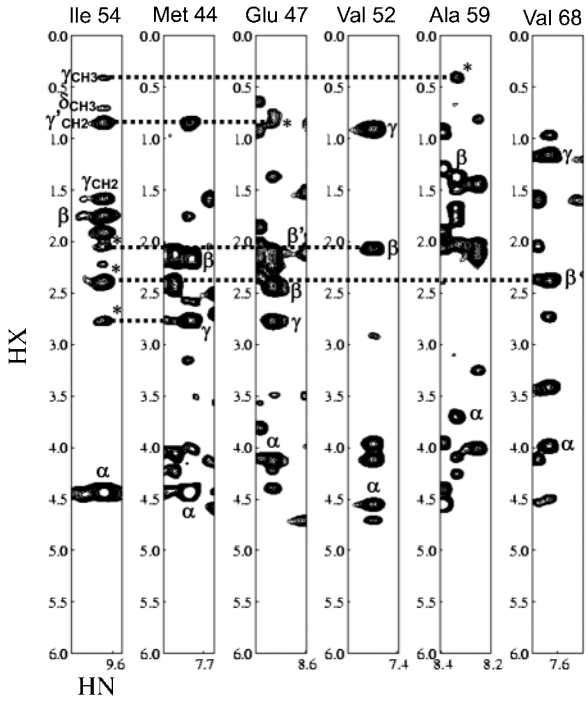

Fig. 9. **3-D ^{15}N-edited NOESY-HSQC spectrum of *H. pylori* ACP at pH 6.** The composite of strips corresponding to residues that exhibit the NOE cross-peaks of Ile 54 is represented. Ile 54 shows correlations with the residues showing a relatively large change in chemical shift perturbation by varying pH. NOE cross-peaks are marked by asterisks.

DISCUSSION

The ACPs are highly conserved in various bacterial strains (*17–21*). The secondary structure of *H. pylori* ACP is composed of three long helices and one short helix, which is similar to those of other ACPs, with minor variations. However, the pH-dependent conformational property of *H. pylori* ACP is unlike that of *E. coli* ACP or *V. harveyi* ACP; at pH 7, *E. coli* ACP adopts a native-like helical conformation and *V. harveyi* ACP adopts a random coil, while *H. pylori* ACP folds like an intermediate conformation between *E. coli* ACP and *V. harveyi* ACP. The random coil-like character of *V. harveyi* ACP was proposed to be originated from a greater negative charge (–2) in loop I and a lack of the histidine residue at position 75 of *E. coli* (*12*). This seems reasonable, since *H. pylori* ACP has the same negativity in loop I as *E. coli* ACP, but the basic histidine is substituted for an asparagine (Fig. 3). Interestingly, a basic lysine is located at the position next to Asn 75, which helps to maintain the structural stability of *H. pylori* ACP compared to *V. harveyi* ACP (*12*, *13*). The detailed examination of the structure of *H. pylori* ACP clearly showed the contribution of Asn 75 and Lys 76 to the structural stability. As shown in Figure 10, hydrophilic Glu 47, Asn 75, and Lys 76 of *H. pylori* ACP are unexpectedly buried in the hydrophobic core in the average structure, which is distinctively different from *E. coli* and *B. subtilis* ACPs. The hydrophobic region of Glu 47 side chain is packed against Val 52 and Ile 54 and the side chain oxygen is directed toward the core, while Glu 47 of the other ACPs is exposed to sol-

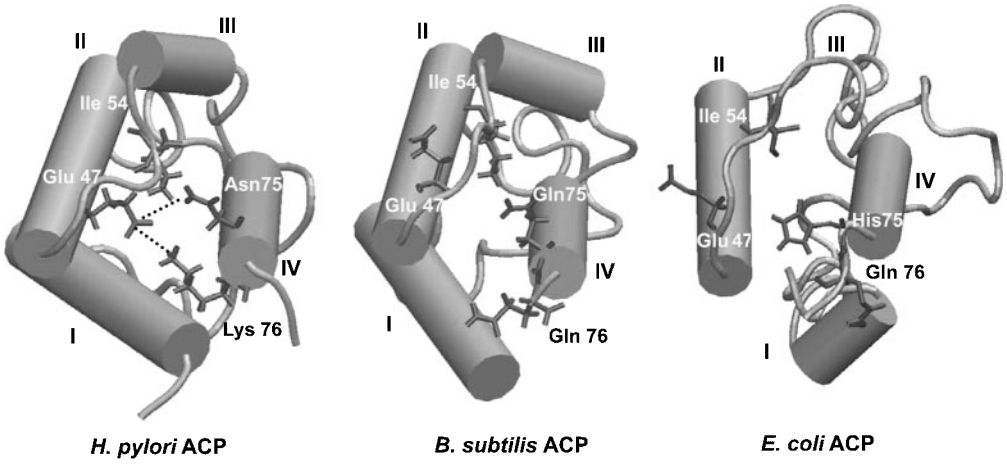

Fig. 10. **Schematic representation showing the buried hydrophilic residues Glu 47, Asn 75 and Lys 76 in the energy minimized average structure of *H. pylori* ACP.** Putative hydrogen-bonding interactions are indicated by dotted lines.

vent. Also, γN protons of Asn 75 interact with amide proton of Glu 47 and methyl protons of Val 52 and Ile 54, which is evidenced by clear long-range NOEs. This brings the Asn (γNH_2) group in close proximity to the Glu 47 (γO) group, allowing the formation of a hydrogen bond. Moreover, the conformation of the side chain of Lys 76, which is mainly maintained by hydrophobic interaction with Leu 3, Lue 46, and Phe 50, shows a possible hydrogen bond donor for the γO of Glu 47. However, ζNH_2 resonances were not observed in NMR spectra, suggesting that Lys 76 may only be weakly hydrogen-bonded. This result could suggest that, unlike *E. coli* and *B. subtilis* ACPs, the helical bundle of *H. pylori* ACP is maintained by not only hydrophobic interactions but also hydrophilic interactions, and by pH elevation these interactions may be weakened because of the increased exchange rate of protons from Asn and Lys side chains. Therefore, the network of Glu 47, Ile 54, Asn 75, and Lys 76 should be very important for the structural stability. The chemical shift changes shown in Fig. 6 are well explained with this correlation.

The altered chemical shift and increased flexibility of Phe 28 also indicate the partial disruption of the hydrophobic core, since the side chain of Phe 28 contacts with the hydrophobic core formed by the packing of the helical bundle (*19*). It is reasonable that this flexibility may assist the acylation of Ser 36 providing an opened environment. The sign of disruption of the helical bundle formation is also reflected in the increased or decreased NOE values of helices I, II and IV (residues Ile 7, Ile 11, Gln 14, Val 15, Leu 42, Ile 43, Leu 46, Gly 66, and Ile 72) (*17–21*). The most interesting point is the changes that occurred around loop II. Ile 54 in this region is very sensitive to pH, revealing the extensive chemical shift variation with decreased flexibility. As shown in Fig. 9 and 10, Ile 54 is important for maintaining the spatial arrangement of helices II, III, and IV. This residue has been previously implicated in interaction with a covalently attached acyl group (*43*). Mutation of Ile 54 in *V. harveyi* ACP showed impaired holo-ACP formation, and this mutant ACP has a greater hydrodynamic radius with incompactness of the conformation (*12*). It may be involved in the binding interface of the ACP-ACPS complex (*23*), which explains the failure of acylation of mutant ACP (I54A) (*12*). Thus, the change of Ile 54 directly indicates the destabilization of the higher order structure. The extensive chemical shift changes should be a result of the structural change, which may be due to the loosened interactions with Glu 47, Asn 75, and Lys 76 described above. Additionally, the migration of Ile 54 seems to provoke a chain movement of helices III and IV, resulting in partial collapse of the compact helical bundle. The disappearing of Asp 56 at pH 7 may be caused by increased flexibility, which, combined with the varied NOE values in the regions F5 and R2 (Fig. 7b), also indicates that helix III would be more easily destroyed by pH alteration. Taken together, our results suggest the destabilization of the ordered structure occurs by denaturation of helices II and III through movement of loop II, accompanied by loss of rigidity of loop I region in the vicinity of helix II. Moreover, this collapse should originate from the disruption of interaction between Glu 47, Ile 54, Asn 75, and Lys 76.

It is well known that binding of divalent metal ions such as Mg^{2+} can stabilize the folding of ACP (*13*, *40*). The putative metal-binding sites are proposed to be Glu 30, Asp 35, Asp 38, Glu 47, Asp 51, Glu 53, and Asp 56 in *E. coli*; and these are well conserved in *H. pylori,* while Glu 30 and Asp 51 are replaced with Lys 30 and Gly 51 (*44*). Notably, these residues are involved in the most variable regions of flexibility described above, indicating the binding of metal ion could be effective in the regulation of flexibility of *H. pylori* ACP at neutral pH.

The variable flexibility of *H. pylori* ACP at different pHs may be related to the diversity of its interaction with various enzymes. As described earlier, the moieties of ACP mediating formation of a complex are different according to its interacting partners, while it is believed helices II and III are the main motif for the binding interface of ACPs (*22–24*). A rigidly ordered structure may not represent the diversity of interaction, to which the presence of a dynamic structure should be of benefit. Thus, it is no accident that the most variable regions of flexibility of *H. pylori* ACP are centralized in the vicinity of helices

II and III, suggesting that the binding specificity of ACPs for a complex formation is probably regulated by a local change of these helices.

This work was supported by National Research Laboratory Program (M1-0203-00-0075) and the 21C Frontier Program (M101KB010001–02K0201–02110) of the Korea Ministry of Science and Technology. This work was also supported in part by 2003 BK21 project for Medicine, Dentistry, and Pharmacy.

REFERENCES

1. Rock, C.O., Jackowski, S., and Cronan, J.E., Jr. (1996) in *Biochemistry of Lipids and Lipoproteins and Membranes* (Vance, E.E., and Vance, J., Eds.) pp 35–74, Elsevier, Amsterdam
2. Tang, L., Weissborn, A.C., and Kennedy, E.P. (1997) Domains of *Escherichia coli* acyl carrier protein important for membrane-derived-oligosaccharide biosynthesis. *J. Bacteriol.* **179**, 3697–3705
3. Issartl, J.-P., Koronakis, V., and Hughes, C. (1991) Activation of *Escherichia coli* prohaemolysin to the mature toxin by acyl carrier protein-dependent fatty acylation. *Nature* **351**, 759–761
4. Shen, B., Summers, R.G., Gramajo, H., Bibb, M.J., and Hutchinson, C.R. (1992) Purification and characterization of the acyl carrier protein of the *Streptomyces glaucescens* tetracenomycin C polyketide synthase. *J. Bacteriol.* **174**, 3818–3821
5. Geiger, O., Spaink, H.P., and Kennedy, E.P. (1991) Isolation of the *Rhizobium leguminosarum* NodF nodulation protein: NodF carries a 4′-phosphopantetheine prosthetic group. *J. Bacteriol.* **173**, 2872–2878
6. Vandem, B.T. and Cronan, J.E., Jr. (1989) Genetics and regulation of bacterial lipid metabolism. *Annu. Rev. Microbiol.* **43**, 317–343
7. Jones, P.J., Holak, T.A., and Prestegard, J.H. (1987) Structural comparison of acyl carrier protein in acylated and sulfhydryl forms by two-dimensional ^{1}H NMR spectroscopy. *Biochemistry* **26**, 3493–3500
8. Rock, C.O. and Cronan, J.E., Jr. (1979) Re-evaluation of the solution structure of acyl carrier protein. *J. Biol. Chem.* **254**, 9778–9785
9. Cronan, J.E., Jr. (1982) Molecular properties of short chain acyl thioesters of acyl carrier protein. *J. Biol. Chem.* **257**, 5013–5017
10. Rock, C.O., Cronan, J.E., Jr., and Armitage, I.M. (1981) Molecular properties of acyl carrier protein derivatives. *J. Biol. Chem.* **256**, 2669–2674
11. Keating, D.H. and Cronan, J.E., Jr. (1996) An isoleucine to valine substitution in *Escherichia coli* acyl carrier protein results in a functional protein of decreased molecular radius at elevated pH. *J. Biol. Chem.* **271**, 15905–15910
12. Flaman, A.S., Chen, J.M., Van Iderstine, S.C., and Byers, D.M. (2001) Site-directed mutagenesis of acyl carrier protein (ACP) reveals amino acid residues involved in ACP structure and acyl-ACP synthetase activity. *J. Biol. Chem.* **276**, 35934–35939
13. Keating, M.-M., Gong, H., and Byers, D.M. (2002) Identification of a key residue in the conformational stability of acyl carrier protein. *Biochim. Biophys. Acta* **1601**, 208–214
14. Kim, Y. and Prestegard, J.H. (1989) A dynamic model for the structure of acyl carrier protein in solution. *Biochemistry* **28**, 8792–8797
15. Mayo, K.H. and Prestegard, J.H. (1985) Acyl carrier protein from *Escherichia coli*. Structural characterization of short-chain acylated acyl carrier proteins by NMR. *Biochemistry* **24**, 7834–7838
16. Holak, T.A., Nilges, M., Prestegard, J.H., Gronenborn, A.M., and Clore, G.M. (1988) Three-dimensional structure of acyl carrier protein in solution determined by nuclear magnetic resonance and the combined use of dynamical simulated annealing and distance geometry. *Eur. J. Biochem.* **175**, 9–15
17. Kim, Y. and Prestegard, J.H. (1990) Refinement of the NMR structures for acyl carrier protein with scalar coupling data. *Proteins* **8**, 377–385
18. Crump, M.P., Crosby, J., Dempsey, C.E., Parkinson, J.A., Murray, M., Hopwood, D.A., and Simpson, T.J. (1997) Solution structure of the actinorhodin polyketide synthase acyl carrier protein from *Streptomyces coelicolo*r A3(2). *Biochemistry* **36**, 6000–6008
19. Xu, G-Y., Tam, A., Lin, L., Hixon, J., Fritz, C.C., and Powers, R. (2001) Solution structure of *B. subtilis* acyl carrier protein. *Structure* **9**, 277–287
20. Roujeinikova, A., Baldock, C., Simson, W.J., Gilroy, J., Baker, P.J., Stuitje, A.R., Rice, D.W., Slabas, A.R., and Rafferty, J.B. (2002) X-ray crystallographic studies on butyryl-ACP reveal flexibility of the structure around a putative acyl chain binding site. *Structure* **10**, 825–835
21. Wong, H.C., Liu, G., Zhang, Y.-M., Rock, C.O., and Zheng, J. (2002) The solution structure of acyl carrier protein from *Mycobacterium tuberculosis*. *J. Biol. Chem.* **277**, 15874–15880
22. Parris, K.D., Lin, L., Tam, A., Mathew, R., Hixon, J., Stahl, M., Fritz, C.C., Seehra, J., and Somers, W.S. (2000) Crystal structures of substrate binding to *Bacillus subtilis* holo-(acyl carrier protein) synthase reveal a novel trimeric arrangement of molecules resulting in three active sites. *Structure* **8**, 883–895
23. Zhang, Y.-M., Rao, M.S., Heath, R.J., Price, A.C., Olson, A.J., Rock, C.O., and White, S.W. (2001) Identification and analysis of the acyl carrier protein (ACP) docking site on beta-ketoacyl-ACP synthase III. *J. Biol. Chem.* **276**, 8231–8238
24. Worsham, L.M.S., Earls, L., Jolly, C., Langston, K.G., Trent, M.S., and Ernst-Fonberg, M.L. (2003) Amino acid residues of *Escherichia coli* acyl carrier protein involved in heterologous protein interactions. *Biochemistry* **42**, 167–176
25. Kyte, J. and Doolittle, R.F. (1982) A simple method for displaying the hydropathic character of a protein. *J. Mol. Biol.* **157**, 105–132
26. Bodenhausen, G. and Ruben, D.J. (1980) Heteronuclear 2D correlation spectra with double in-phase transfer steps. *Chem. Phys. Lett.* **69**, 185–189
27. Ikura, M., Bax, A., Clore, M., and Gronenborn, A.M. (1990) Detection of nuclear Overhauser effects between degenerate amide proton resonances by heteronuclear three-dimensional nuclear magnetic resonance spectroscopy. *J. Amer. Chem. Soc.* **112**, 9020–9021
28. Gronenborn, A.M., Bax, A., Wingfield, P.T., and Clore, M. (1989) A powerful method of sequential proton resonance assignment in proteins using relayed ^{15}N-^{1}H multiple quantum coherence spectroscopy. *FEBS Lett.* **243**, 93–98
29. Kay, L.E. and Bax, A. (1990) New methods for the measurement on NH-Ha coupling constants in ^{15}N labeled proteins. *J. Magn. Reson.* **86**, 110–114
30. Kay, L.E., Ikura, M., Tschudin, R., and Bax, A. (1990) Three-dimensional triple resonance NMR spectroscopy of isotopically enriched proteins. *J. Magn. Reson.* **89**, 496–502
31. Wittekind, M. and Mueller, L. (1993) HNCACB, a highsensitivity 3D NMR experiment to correlate amideproton and nitrogen resonances with the α-carbon and β-carbon resonances in proteins. *J. Magn. Reson. ser. B* **101**, 214–217
32. Grzesiek, S. and Bax, A. (1992) Correlating backbone amide and side-chain resonances in larger proteins by multiple relayed triple resonance NMR. *J. Amer. Chem. Soc.* **114**, 6291–6293
33. Wishart, D.S., Bigam, C.G., Yao, J., Abildgaard, F., Dyson, H.J., Oldfield, E., Markley, J.L., and Sykes, B.D. (1995) ^{1}H, ^{13}C and ^{15}N chemical shift referencing in biomolecular NMR. *J. Biomol. NMR* **6**, 135–140
34. Delaglio, F., Grzesiek, S., Vuister, G.W., Zhu, G., Pfeifer, J., and Bax, A. (1995) NMRPipe: a multidimensional spectral processing system based on UNIX pipes. *J. Biomol. NMR* **6**, 277–293
35. Wüthrich, K. (1986) *NMR of Proteins and Nucleic Acids*, John Wiley & Sons, New York
36. Wishart, D.S. and Sykes, B.D. (1994) The ^{13}C chemical-shift index: a simple method for the identification of protein second-

ary structure using ^{13}C chemical-shift data. *J. Biomol. NMR* **4**, 171–180
37. Park, S.J., Kim, J.-S., Son, W.-S., Ahn, H.-C., and Lee, B.J. (2003) *J. Biochem. Mol. Biol.* in press
38. Reid, D.G. (1997) *Protein NMR Techniques*, Humana Press, Totowa, New Jersey
39. Cornilescu, G., Delaglio, F., and Bax, A. (1999) Protein backbone angle restraints from searching a database for chemical shift and sequence homology. *J. Biomol. NMR* **13**, 289–302
40. Schulz, H. (1975) On the structure-function relationship of acyl carrier protein of *Escherichia coli*. *J. Biol. Chem.* **250**, 2299–2304
41. Horvath, L.A., Sturtevant, J.M., and Prestegard, J.H. (1994) Kinetics and thermodynamics of thermal denaturation in acyl carrier protein. *Protein Sci.* **3**, 103–108
42. Garrett, D.S., Seok, Y.J., Liao, D.I., Peterkofsky, A., Gronenborn, A.M., and Clore, G.M. (1997) Solution structure of the 30 kDa N-terminal domain of enzyme I of the *Escherichia coli* phosphoenolpyruvate: sugar phosphotransferase system by multidimensional NMR. *Biochemistry* **36**, 2517–2530
43. Jones, P.-J., Cioffi, E.A., and Prestegard, J.H. (1987) (^{19}F)-^{1}H heteronuclear nuclear Overhauser effect studies of the acyl chain-binding site of acyl carrier protein. *J. Biol. Chem.* **262**, 8963–8965
44. Frederick, A.F., Kay, L.E., and Prestegard, J.H. (1988) Location of divalent ion sites in acyl carrier protein using relaxation perturbed 2D NMR. *FEBS Lett.* **238**, 43–48